

An experimental test of the critical behaviour of fracture precursors

A. Guarino, A. Garcimartín^a, and S. Ciliberto^b

Laboratoire de Physique, École Normale Supérieure de Lyon, 46 allée d'Italie, 69364 Lyon Cedex 07, France

Received: 23 January 1998 / Revised: 20 April 1998 / Accepted: 17 June 1998

Abstract. The statistical properties and the localization of fracture precursors on heterogeneous materials is studied by recording their acoustic emission as a function of the applied load. It's found that the microcrack cluster together as the load increases and the instantaneous acoustic energy has an invariant power law distribution. The integrated acoustic energy presents a critical divergency close to the failure load for the sample. These result support the idea that fracture can be viewed as a critical phenomenon. Finally a measure of the concentration of microcracks, which allows us to predict the failure load, is introduced. These properties are studied also when a periodic load is applied to the sample. It's found that the Kaiser effect is not strictly satisfied in heterogeneous materials.

PACS. 62.20.Mk Fatigue, brittleness, fracture, and cracks – 46.30.Nz Fracture mechanics, fatigue, and cracks – 81.40.Np Fatigue, corrosion fatigue, embrittlement, cracking, fracture and failure

1 Introduction

Crack propagation in solid materials and its prediction are very important subjects from a technological point of view [1–3]. Traditionally, uncertainties and lack of knowledge were taken into account in “safety factors”. However these two subjects have always received a lot of attention because a better understanding of fracture will certainly improve the design of mechanical systems. This interest comes not only from engineers but also from the physics community, who more recently began to face fundamental questions concerning the basic mechanisms and processes involved in fracture [5]. Among the fundamental problems recently studied one can mention the appearance of dynamical instabilities in the fracture propagation [6], the statistical description of microcracks [7], and the study of scaling laws of the roughness of the fracture surfaces [8,9]. The most important question, which has not yet been solved in general, is the prediction, starting from first principles, of the critical load needed to break a sample. The case of heterogeneous materials is a special one. Indeed the Griffith criterion [1,2] for a crack is derived from first principles but the presence of defects in the materials may change considerably the load needed to break the material. Thus it is not surprising that many different analytical [10] and numerical approaches have being explored, such as for example molecular dynamics [11–14] and fuse networks [15,16].

The effort to provide conceptually simple models of fracture [17] is particularly valuable. Among those models, percolation theory and self-organized criticality [18] stand out. While they often fail to reproduce in detail the complex phenomenology observed they can nevertheless provide meaningful insights. Comparison with experiments is difficult, because of the inherent simplifications assumed in the models. However qualitative features should be amenable to experimental testing. Some results in this direction were presented in a recent letter [19]. The main motivation of our work is to try to investigate whether these models reproduce the main characteristics of the fracture process. In particular, we focus on the description of the fracture as a critical phenomenon [20–23], as revealed, for instance, by the behavior of a characteristic parameter of the system near failure. Here we discuss this point and we provide experimental data to support it.

To do this, our main tool is the monitoring of the acoustic emission (AE) from microfractures that occur before the final crack. Two things are obtained from the signal. The first one is the position of microcracks. The technique has been widely used in seismography, and to map the nucleation and development of fractures. The second one is the energy of the sound waves. This is a good parameter to compare with the mentioned models: energy will be one of the characteristic parameters of the system when studying the critical character of fracture.

The paper is organized as follows. In the next section, we describe the experimental setup. In Section 3, we present the results concerning the localization of microfractures. In Section 4, starting from the energy

^a *Permanent address:* Departamento de Física, Facultad de Ciencias, Universidad de Navarra, 31080 Pamplona, Spain.

^b e-mail: ciliberto@physique.ens-lyon.fr

measurements, we discuss why and how fracture can be viewed as a critical phenomenon. In Section 5, we briefly discuss the Kaiser effect. Finally, some conclusions are gathered in Section 6.

2 Experimental setup and procedures

The experiment was designed to obtain the energy and position of microfractures from their AE. Usually the apparatus employed in other fracture experiments involve moving parts and electric motors that introduce a lot of noise both acoustic and electric. Low noise is very important to have a large dynamic range of energy events. We have built an electrically shielded setup without moving parts. It consists basically of two chambers between which the sample is placed; pressurized air is injected in one chamber, and the pressure difference supported by the sample is the force that breaks it.

2.1 The samples

Several materials have been used. Most of the runs have been carried out on two fibrous composite materials: chip-board wood panel, which is made of small wood fibers randomly oriented, and different fiberglass panels made of a fiber fabric and an epoxy resin. Samples are circular, having a diameter of 22 cm, and a thickness of several millimeters (typically 5 mm for wood panels, and 3 mm for fiberglass). The Young modulus of the samples is 1.8×10^8 N/m² and 10^{10} N/m² for the wood panels and the fiberglass respectively. The longitudinal sound velocity is 1900 m/s for wood panels and 2200 m/s for fiberglass. The choice of the materials was determined by their features: they consist of small fibers, randomly oriented, and they are elastic and heterogeneous.

2.2 The apparatus

The mechanical arrangement is composed by a metallic cylindrical chamber with the sample closing the top side (see Fig. 1). The inner diameter of the chamber is 20 cm and its height is of 10 cm. To make the cavity airtight an O-ring is placed between the sample and the chamber end a second piece that fixes the sample in place is screwed. A thin film of polyethylene is glued on the sample if the material is porous. The force needed to stretch this plastic is much smaller than the force supported by the sample. Another metallic cylindrical piece covers the upper side of the sample. It provides electric shield and protects from projections when the sample breaks. The upper chamber is at the atmospheric pressure. Pressurized air is slowly injected in the bottom chamber. The time needed to break a sample is typically 2 hours, but it can be changed from 10 minutes to 5 hours in order to study the dependence of the result on the loading rate.

Pressure is monitored by a differential solid-state pressure sensor which measures the pressure difference

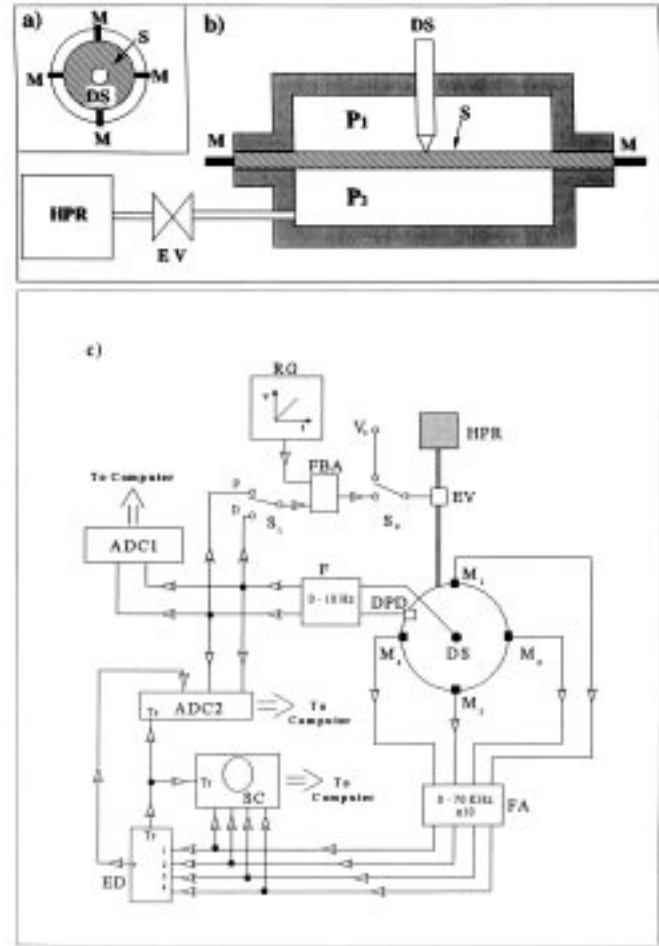


Fig. 1. Sketch of the apparatus. (a) Top view. S: sample; DS: displacement sensor; M: microphones. (b) Side view. HPR: high pressure reservoir, E: electronic valve. The pressure supported by the sample is $P = P_2 - P_1$. (c) Outline of the acquisition system. The signals from a differential pressure transducer (DPD) and a displacement sensor (DS) are low-pass filtered at 10 Hz in F, then sent to an analog to digital converter (ADC1). The AE is detected by four microphones M1-M4, low-pass filtered at 70 kHz and amplified in FA, then sent to an oscilloscope SC and to an electronic device ED that integrates the sum of the squared amplitudes during a time window of 30 ms. The result is sent to the analog to digital converter ADC1. The device ED also sends a trigger to SC and ADC2 each time that one of the signals from M1-M4 goes above a fixed level. The electronic valve EV controls the air flow from a high pressure reservoir HPR. It is controlled by a feedback loop FBA that compares a ramp generated at RB with the signal P or D selected by switch S1. Feedback can be disabled at switch S2 so that EV imposes a constant flow.

$P = P_2 - P_1$ between the two chambers. The resolution of this measurement is 0.002 atm. Typical fracture pressures are of the order of 1 atm. The deformation at the center of the sample is recorded with an inductive displacement sensor (Linear Differential Variable Transformer 500 HR from PM Instruments). The accuracy of the position measurement is 10 μ m. Just before fracture, the deformation

at the center of the sample is typically of a few centimeters. The weight of the sensing element, which rests on the sample, is just 25 g, so it is negligible when compared to the force exerted by the pressurized air.

The pressure difference is established by means of a feedback loop and an electronically controlled valve (model 248A from MKS Instruments). This valve connects the bottom chamber with a pressurized air reservoir, and can control flows of up to 200 cm³/min with a precision better than 0.1%, allowing us for both a short response time and slow loading. The feedback loop can control either the pressure or the displacement. Thus the sample can be loaded at imposed stress or at imposed strain. This is obtained by comparing in the feedback electronics either the pressure or the displacement signal with a reference ramp that increases linearly in time. The slope of the ramp, which is set manually, determines the increasing rate of the control parameter (the pressure or the displacement). Finally, by switching off the feedback loop and imposing a constant voltage to the valve, one can load the sample at imposed flow, *i.e.* by imposing neither the pressure nor the displacement but by supplying a constant air flow to the bottom chamber (see Fig. 1). When the feedback is on, the chosen control parameter of the experiment is strictly regulated. Largest deviations from the reference ramp are smaller than 1% and quickly corrected (the characteristic time of the system is of about 0.1 s).

Four microphones (wide-band piezoelectric detectors Pinducer VP-1093 by Valpey-Fisher) are used to record the AE. They are screwed into holes made in one of the metallic pieces (see Fig. 1). The acoustic contact between the microphones and the sample is ensured by a thin layer of honey.

The acquisition system is shown in Figure 1c. An analog to digital converter (ADC1), connected to the controlling computer, captures continuously in time (at 8 points per second) the pressure difference and the displacement to produce the load curve. The signals detected by the four microphones are amplified and low-pass filtered at 70 kHz to reduce noise and the filtered signals are sent to a four channel digitizing oscilloscope (Tektronix TDS 420) and to an electronic device ED. Notice that above 60 kHz the amount of AE from the microcracks is negligible, in the materials we used. This has been checked because our detectors and electronics have a full bandwidth of 2 MHz and above 60 kHz the amount of AE is negligible. The electronic device ED is used to trigger one acquisition when the signal from any microphone goes over a fixed level. The trigger level is set just above the noise level. The oscilloscope is programmed to capture the four waveforms detected by the microphones, and to send them to the controlling computer, which arms again the oscilloscope once the transfer is complete. The maximum transfer rate is 1.52 events per second. The electronic device ED also performs the sum of the square of the AE amplitude detected by each microphone and integrates it over a time window of 30 ms, which is longer than the duration of acoustic events (typically in the range 2-4 ms). The output is an analog signal ε proportional to the

energy of the AE. This signal, with those of instantaneous pressure and displacement, are sent to another analog to digital converter (ADC2), and stored till the end of the run. Only 0.5 ms are needed for each transfer; the device is then automatically armed. Therefore, only a small fraction of the energy may eventually be lost. The gain of the energy measurement system has been adjusted to provide the largest possible dynamic range, between the final, strongest crack, which is the only one that may saturate the device, and the trigger level just above the noise. The ratio between the energy of the biggest and of the smallest detected events is about 10^{-4} .

2.3 Acoustic data analysis

In Figure 2 we show a typical AE signal from a microfracture. The arrival time of these signals are used to compute the position of the recorded microfractures at the end of each experiment. This is done in the following way. First, from the AE signals acquired by the oscilloscope, the arrival time to each microphone is obtained. We have used several schemes to find the point where the signal goes out of the noise level. For example, one criterion was based on the deviation of the amplitude from the mean, and another on the integration of the absolute value of the amplitude to find the beginning of the signal. All these algorithms give the arrival time with a precision of about $\pm 1.5 \mu\text{s}$. With these data and the sound velocity, which we measured in several samples (see Sect. 2.1), the program finds the location of microfractures. This is done in a recursive way by successive approximations. The algorithm finds the location that minimizes the difference between the measured arrival time to each microphone, and the calculated arrival times of the position considered by the program. The mean standard deviation for the calculated positions is ± 3 mm. This comes mainly from uncertainties in the detection of the arrival time. We are not able, however, to find the position of every single microfracture that triggers the acquisition system. For some of them, for example, the uncertainty in the position is large and they are rejected. A small fraction, about 1% of the total number of microcracks, comes from outside the sample, and are caused by external noise. The amplitudes of these events, produced by noise, is very weak, and their contribution to the total acoustic energy can be neglected. Finally, if events occur at a faster rate than the data transfer capability, some waveforms are lost, although their energy is recorded by ED. As a result, we are normally able to locate about half of the detected microfractures. Their number spans from 500 to 3000, depending on the material.

The fact that the signal at the output of the electronic device is proportional to the energy of AEs is strictly true only if there is no sound attenuation in the material. We have measured the attenuation coefficient and we concluded that events coming from different positions give almost the same energy signal. Variations in the measured energy are in the worst case 7% in fiberglass samples, 5% for wood and even smaller for plaster. As many microfractures come from the central zone of the sample,

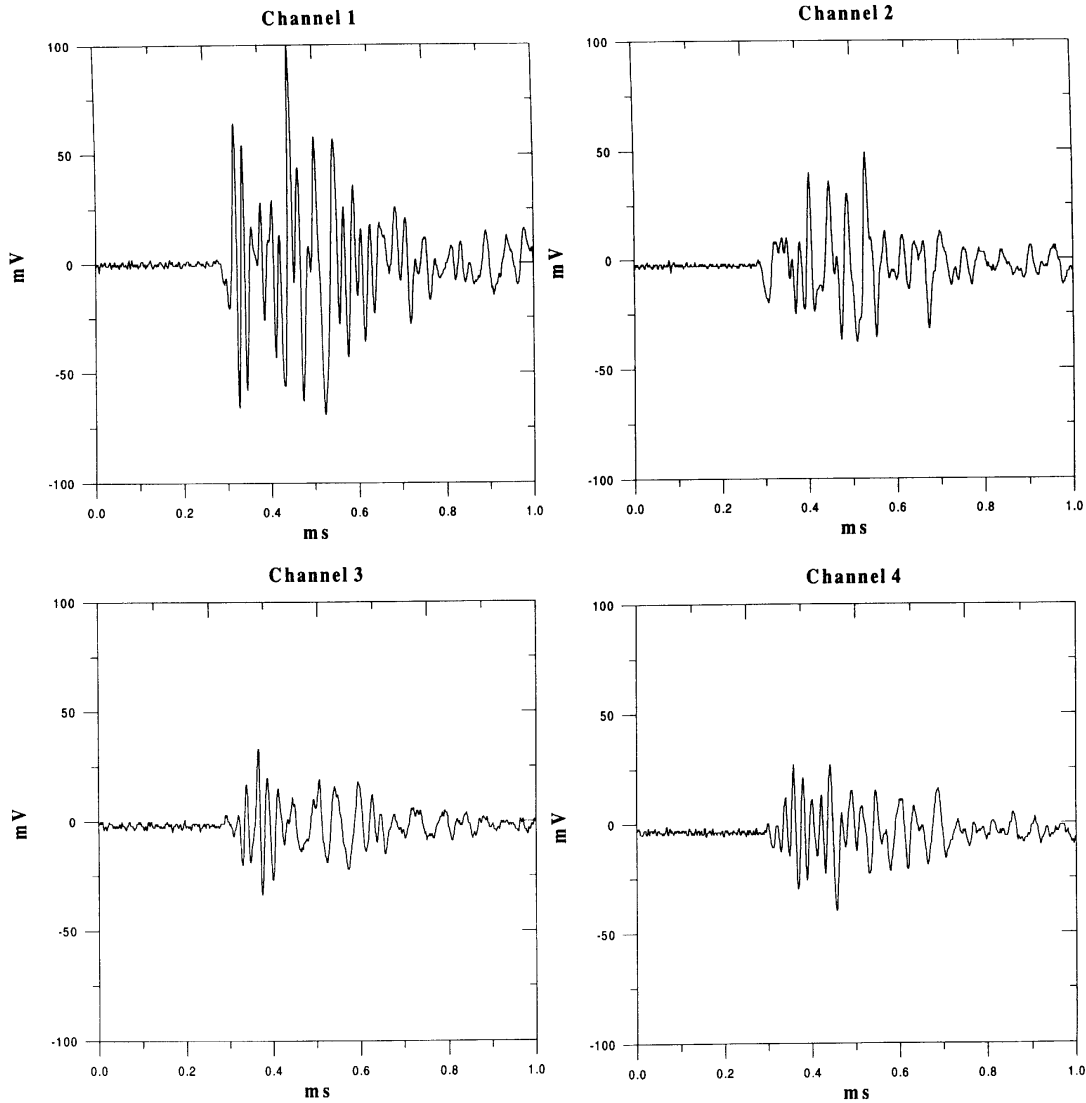


Fig. 2. AE signal captured by the oscilloscope. Each waveform corresponds to one microphone (channel).

this figure should be typically much smaller. Besides, no angular pattern is observed in the AE. Although microcracks usually emit as a dipole [24] or as a quadrupole [25], in our case the wavelength (of the order of some centimeters) is much larger than the source size; therefore, it is expected that diffraction of sound waves removes any directionality. This is also found empirically. After inspecting several hundreds of microfractures from one run, we found that in 62.6% of the cases the biggest amplitude was detected by the nearest microphone (as in Fig. 2), in 34.3% of the cases the amplitudes were approximately equal and only in 3.1% of the cases the strongest amplitude was detected by a microphone other than the nearest. In the last cases, the amplitude difference was very small. For the events taking place at the center of the sample, all microphones detect similar amplitudes. Given this two facts – the absence of directionality and the weak attenuation – we have not taken into account the position of microfractures to calculate their energy.

2.4 Fracture mode and load procedures

Near fracture, the displacement at the center of all the samples we used, is bigger than their thickness. In this case, flexion can be neglected [4, 26]. It can be considered that the plate is stretched from the borders, in a traction with circular symmetry. Therefore as soon as the displacement of the plate center is bigger than sample thickness the fracture mode is mainly the mode I. Of course this does not exclude the possibility that there is a small contribution of a mode II and III.

In our experiments the load procedure is of utmost importance. Our control system allows us to load the sample under sharply regulated conditions. To illustrate the difference between loading the sample at imposed stress or strain, we show in Figures 3a and 3b the loading curve of a sample of wood loaded at imposed pressure and of a sample of wood loaded at imposed displacement respectively. Finally Figure 3c corresponds to a sample

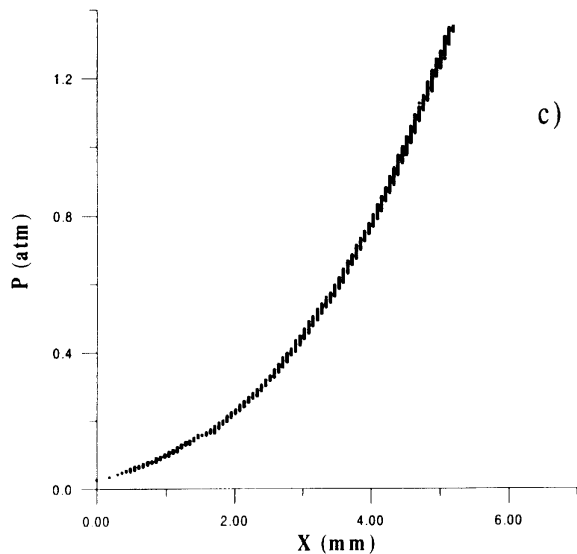
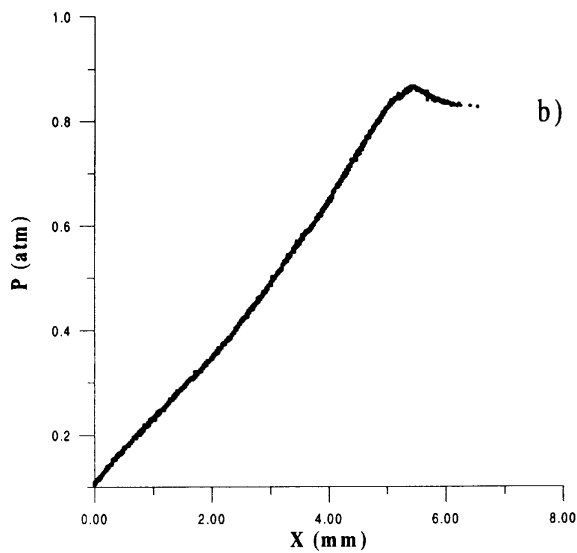
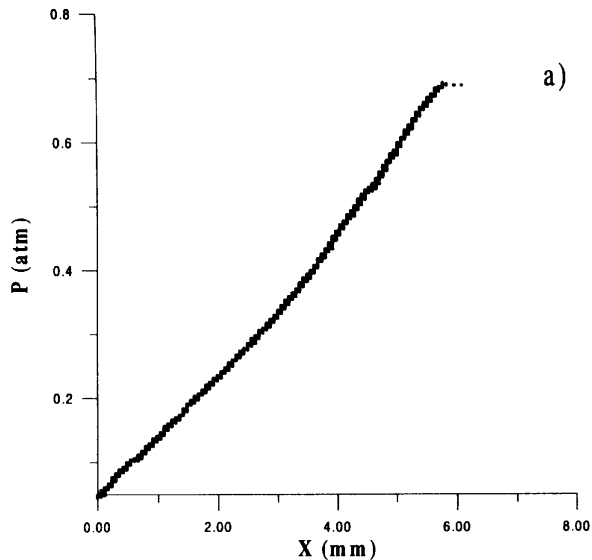


Fig. 3. Load curves of three samples: (a) wood sample at imposed stress; (b) wood sample at imposed strain; (c) fiberglass sample at imposed stress.

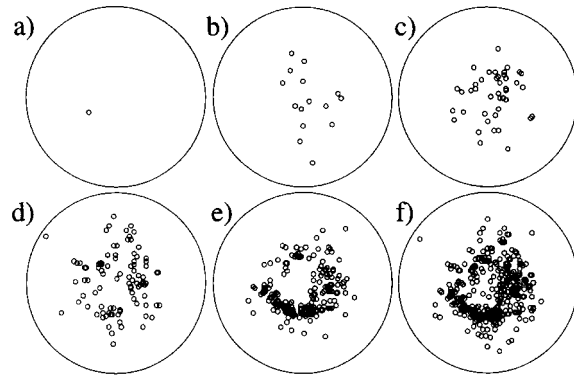


Fig. 4. The localization of microfractures as p is increased. The critical pressure P_c has been divided in five equal pressure intervals. Microfractures detected in each interval are represented in plots (a) to (e) (increasing pressure). In (f) all the microfractures are plotted.

of fiberglass loaded at imposed pressure. We notice immediately the very different behaviour for the wood plates between the imposed strain and the imposed stress procedures. The latter is characterized by an almost linear behaviour till the fracture point. In contrast the imposed strain procedure presents a plastic behaviour induced by damage. Finally the fiber glass load curve (Fig. 3c), is strongly non-linear and the material becomes stronger at high stress. This is due to the fact that the resin in which fibers are embedded deforms first and then the fibers support the applied stress.

3 Localization of microfractures

The acquired data allows us to examine the details concerning the appearance and localization of microcracks. A “movie” of the run can be replayed by representing on a computer display the position of microfractures as P is increased. We call P_c the pressure at which the sample breaks. To give an idea of the image that we get, the pressure interval $[0 \div P_c]$ has been divided in five equal intervals. The microfractures recorded during each of the five intervals are plotted in Figures 4a to 4e. As P is increased, more and more microfractures appear in the sample. It should be noticed that if pressure is decreased before reaching the critical load, and then the sample is loaded again, only a small number of microfractures are detected before attaining the previous maximum load: this is the Kaiser effect [27] (see also Sect. 5).

An interesting feature is observed in the sequence shown in Figure 4. At the beginning, microfractures are roughly uniformly distributed. Afterwards, they begin to concentrate and to nucleate, eventually producing a major fault. Final failure takes place in these nucleation sites. This had already been observed experimentally by Lockner *et al.* [27,28] in granite samples. They distinguish three stages in the process: randomly distributed microfractures,

nucleation, and growth of the nucleation sites. The concentration of microfractures can therefore be a good indicator that the sample is approaching failure. In our experiment, this feature has been quantified.

Several measures of disorder and localization that can be applied to our experiment have been proposed [29,30]. One of them, for example, is the mean segment length of the minimal spanning tree linking all the microfractures occurring in each pressure interval. Nevertheless, this method does not prove satisfactory because of the slow convergence of this quantity with the number of nodes, which follows a square root law. More sophisticated approaches, such as computing the minimal spanning tree of all possible subsets having a fixed number of microfractures and taking the smaller one – which has been successfully used [31] in other situations – could provide a better measure.

The best and simplest method among those we have tested is to calculate the entropy of the distribution of microfractures. To do this the interval of pressure $[0 \div P_c]$ is divided in equal intervals. For each pressure interval a grid is drawn on the surface of the sample and the number of microfractures occurring in each square of the grid n_i is evaluated. Then the entropy is calculated as defined by Shannon: $S = -\sum_i q_i \ln q_i$, where q_i is the probability of occupation of a given square, *i.e.* $q_i = n_i/N$, N being the total number of microfractures in the pressure interval. This quantity depends on N , and therefore it must be normalized to allow comparison between pressure intervals with different N . The normalized entropy is $s = S/S_e$, where S_e is the equipartition entropy, calculated for N microfractures evenly distributed through the sample. Both the grid size and the pressure interval must be chosen so that they contain a significant number of microfractures. We have usually taken between 10 and 20 pressure intervals, and between 80 and 300 grid squares. It should be noticed that the sample can be considered two-dimensional because the thickness is in all cases smaller than the square size. We have checked that the features of s do not depend on these two parameters. The two extreme values $s = 1$ and $s = 0$ correspond, respectively, to a totally disordered set of microfractures and to the concentration of all microfractures in one grid square. The analogous physical situations are a gas and a crystal.

The results obtained for two typical samples of wood are shown in Figure 5a, where s is plotted *versus* normalized pressure $p = P/P_c$. The dashed line is a linear fit. At small values of p the value of the localization entropy s is close to 1 (for values of p smaller than 0.2 there is not a sufficient number of microfractures to calculate the entropy). The decrease of s is similar from one sample to another. Besides, it does not depend on the loading procedure. In fact, one of the samples shown has been broken imposing the pressure and the other imposing the displacement. This is not surprising, since in elastic materials the loading schemes play an important role only very close to the fracture.

The entropy here defined could be used to forecast the critical load. For example, when s goes below $s = 0.75$

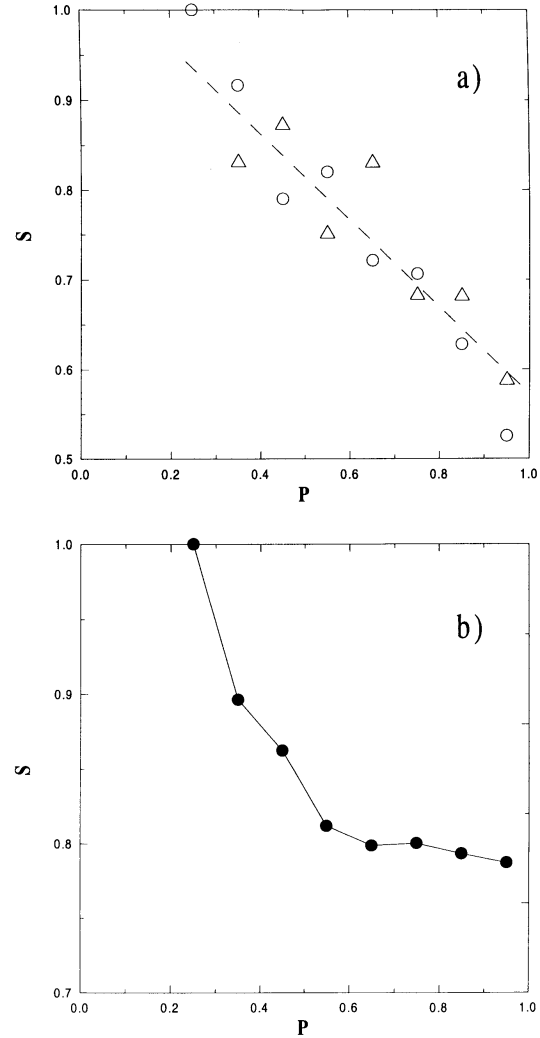


Fig. 5. (a) Normalized entropy s versus normalized pressure p for two wood samples. One of them (circles) is loaded at imposed pressure, and the other (crosses) at imposed displacement. The dashed line is a fit for 20 wood samples. (b) Normalized entropy s versus normalized pressure p for a sample of fiberglass.

it can be stated that P is over 0.6 the critical value with an error of 20%. Two remarks should be done concerning these figures. First of all, the definition of entropy that we have used, although normalized for the number of events, still has a dependence on the grid size, namely, it depends on $\log(K)$, where K is the number of squares of the grid. The aspect of the curve, however, remains the same. This dependence can be removed by using other definitions of entropy. We have kept the simplest one to illustrate the method. Secondly, entropy does not go to zero near failure because microfractures concentrate along a line, not around a point.

The entropy s also displays a decrease in other materials, but the law is different in each case. In Figure 5b the values obtained for a typical sample of fiberglass are shown. It is seen that s decreases sharply at the beginning and afterwards it remains approximately constant.

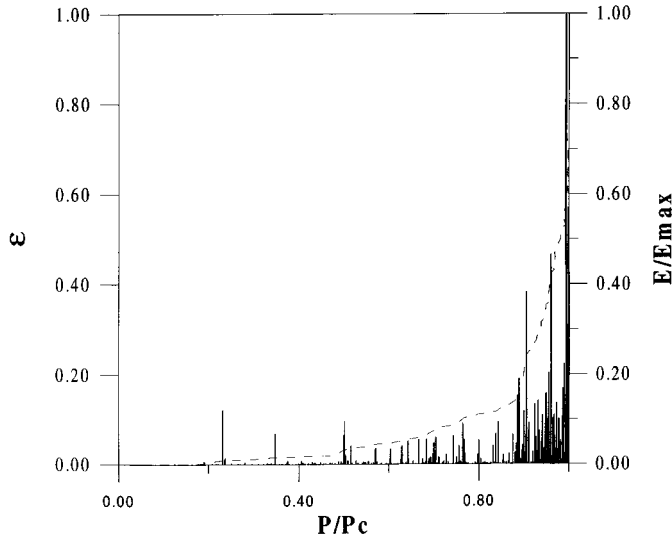


Fig. 6. Energy bursts from AE (arbitrary units) recorded in one wood sample. The dashed line is the cumulated energy E normalized to E_{max} (maximum cumulated energy).

This can be explained as follows. As we discussed in Section 2.4, the load curve (see Fig. 3c) indicates that the material is tougher at the end than at the beginning of the test. Fiberglass plates consist of glass fibers embedded in a resin. When they are loaded, the weakest component (the resin) breaks first, and then fibers begin to crack at the places where resin has given up. Analyzing the entropy we conclude that the nucleation of defects takes place during the first stage; afterwards, events do not further concentrate. It seems plausible that for other materials the behavior of s will be very similar, exhibiting a decrease which is the signature that microfractures are concentrating around the sites where the final crack will develop. This seems to be a good way to assess damage.

4 The behaviour of the released energy

We now turn to energy measurements. The output signal ε of ED of Figure 1 is proportional to instantaneous AE energy. The energy ε recorded in a sample is shown in Figure 6 as a function of P/P_c . In general, each burst corresponds to one microfracture. Nevertheless, it can not be asserted that each microfracture corresponds to the breaking of one bond at a microscopic level. Maybe several bonds break in avalanche. Moreover, it is likely that the strength of each bond is different. This is the reason why we take energy as a characteristic parameter of the system. Although one could be tempted simply to take into account the number of events, it is not a well-defined variable. Because of this, energy (and in particular, energy from AE) was the variable of choice when studying experimentally many related situations: the fracture of granite [28], the acoustic emission from volcanoes [32], chemically induced fracture [33], the fracture of plaster samples cracked by piercing through them [34], and the explosion of an spherical tank [35].

An interesting model that has been proposed for these situations is the fuse network [16]. One aspect that is captured in this model is time dynamics of the redistribution of the load as bonds are broken. In the fuse network, a current is imposed between the two sides of the lattice. When a fuse burns out, the current is redistributed. Scaling laws are found near the total breakdown of the network. The analogy between the variables in the fuse network model and in the fracture experiment is the following: the electric current is formally equivalent to the applied stress; the voltage across the lattice, to the strain; and the conductivity, to the Young modulus. In order to compare the model with fracture experiments, it is crucial to load the sample at imposed stress, and this is the reason for the stringent control of pressure in our setup.

Critical behavior is displayed by the divergence of the characteristic parameter of the system as the control parameter is increased. This is valid only near the critical point, *i.e.* near P_c . In contrast, other phenomena, such as relaxation or saturation, are normally associated to an exponential behavior. We then search a power law for the energy as a function of the reduced control parameter $\frac{P_c - P}{P_c}$. As ε is an intermittent variable, we prefer to use

as susceptibility the cumulated energy $E(P)$ up to a pressure P , that is $E(P) = \int_0^P \varepsilon(P') dP'$. The cumulated energy $E(P)$ is plotted as a function of P in Figure 7. Notice the strong increase of $E(P)$ when P_c is approached. In order to check the critical divergence of $E(P)$ near P_c , $E(P)$ is instead plotted in Figure 7 as a function of the reduced parameter $\frac{P_c - P}{P_c}$ in log-log scale. Figure 7a corresponds to an experiment done at imposed pressure, Figure 7b to an experiment at imposed strain. We immediately see that a critical divergency is observed only for the experiment at imposed pressure. In Figure 7a the continuous straight

lines correspond to the fit $E = E_0 \left(\frac{P_c - P}{P_c} \right)^{-\alpha}$. Both α and P_c are adjustable parameters. In this way the value estimated for P_c is more accurate than that obtained from the loading curve. The values of P_c estimated from the fit and from the loading curve differ of 0.4% at most. We find that for wood panels, $\alpha = 0.27 \pm 0.05$, and for fiberglass $\alpha = 0.22 \pm 0.05$. Notice that the values for the critical exponent, if $\varepsilon(P)$ (and not the cumulated energy) is considered, are $\alpha = 1.27$ and $\alpha = 1.22$ respectively for wood and fiberglass. The values are consistently reproduced in different samples of the same material. Because the measurement incertitude we are not able to say if the exponents are the same or not. The dependence of the critical exponent on the material would be not surprising, since it is influenced by factors such as the type of the bonds, even in numerical models. As we do not have access to the microscopic structure of the material, we are not able to compare this figures to the values obtained for one particular model. Besides, fracture could fall among some systems whose description lies midway between standard percolation and directed percolation [36]. The critical exponent

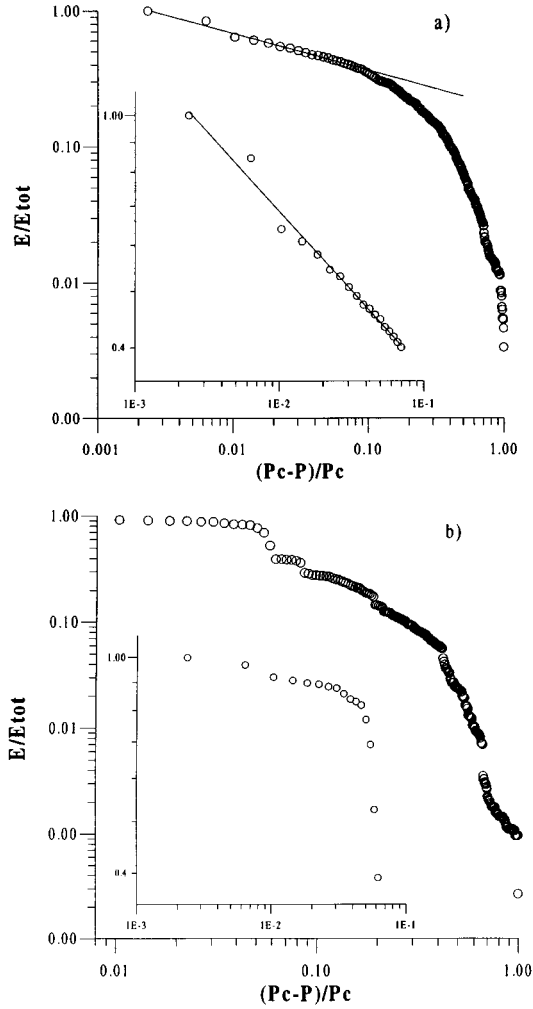


Fig. 7. Cumulated energy E normalized to E_{max} as a function of the reduced control parameter $\frac{P_c - P}{P_c}$ at the neighborhood of the critical point. (a) Case of imposed pressure. The circles are the average for 10 wood samples. The solid line is the fit $E = E_0 \left(\frac{P_c - P}{P_c}\right)^{-\alpha}$. (b) Case of imposed strain. The circles are the average for 5 wood samples. The insets in (a) and (b) are a zoom near P_c .

found depends on features of the system such as the distribution of defects, hence it may change from one case to another. In our opinion, the essential point is that a power law divergence is observed. This supports a description of fracture based on those models.

It is important to stress that the load procedure is paramount to find this. If strain, instead of stress, is imposed, this critical behavior is not found, as can be seen in Figure 7b. This is revealed by the absence of a good power fit, *i.e.*, the characteristic parameter of the system does not diverge at the critical point. It is easy to understand the reason of the difference between the behaviours of the sample submitted to the two different loading procedures. When microfracture occurs the material is damaged to a certain degree and it yields a little. If pressure is imposed, the same load must be endured by the other bonds: the same load is simply redistributed. Therefore it is likely

that other bonds will break as a follow-up. This mechanism may easily trigger an avalanche. Now if displacement is imposed, the material will yield; then the feedback system will feel that strain is too high and will stop increasing the pressure to compensate for it. A smaller load is therefore supported by the sample. A microfracture may then have a stabilizing effect, because the material relaxes by releasing some amount of energy. Note that in our case we do not strictly impose strain if the relaxation is too large. The displacement at the center still departs from a ramp near fracture. To control this properly, pressure should be decreased, and this would involve significant complications in the experiment. It is likely that the absence of a critical exponent would be even more patent if this is done. Finally, if flow is imposed critical behavior is not found either. This is an intermediate situation between imposed stress and imposed strain: in this case the product PV (where V is volume of air) is imposed and the system arranges itself to choose the stress and the strain. It seems clear that fracture can be described as a critical phenomenon only if stress is imposed. This should be emphasized since many fracture experiments and tests are done at imposed strain.

More knowledge about the fracture process can be obtained by examining the histogram of the energy released by microcracks. In many related situations, a power distribution is obtained, such as the Gutenberg-Richter law for earthquakes [37,38], where the exponent for the distribution of the released energy is about -1.5 , or in the avalanche magnitudes in the model of self-organized criticality [18]. Interestingly, this has also been found in a numerical simulation of the fracture of a bundle of fibers [39], which may be more closely related to our case. In our experiment, we observe that the energy released displays this statistics as well: $N(\varepsilon) \propto \varepsilon^{-\gamma}$ (see Fig. 8a). Where $N(\varepsilon)$ is the number of events with a given energy ε . The exponent found is $\gamma = 1.51 \pm 0.05$ for wood, and $\gamma = 2.0 \pm 0.1$ for fiberglass. An interesting point concerning this numbers is that we do not appreciate any variation when changing the loading conditions as described above. We would like to emphasize, however, that the exponent of the power law distribution is not constant during the run (the figures provided are for all the events taken together). This has been observed also by Lockner [28]. Lockner has associated different exponents to the stages of prenucleation, nucleation and growth of the main crack. We observed that the exponent at the first stages of the run, is a little bit larger than at the end but, due to the smaller number of events detected in each run, we are at the limit of the measure incertitude and we are not able to refine our results to the same point, but they seem to confirm that. We have also studied the distribution $N(\tau)$ of the time interval τ between events. The result of this analysis is show in Figure 8b where $N(\tau)$ is plotted as a function of τ . We clearly see $N(\tau)$ has a power law dependence on τ . Specifically, $N(\varepsilon) \propto \tau^{-\beta}$ with $\beta = 1.9 \pm 0.1$ for wood and 2.7 ± 0.1 for fiberglass. The distribution do not depend on the threshold we used. The fact that γ depends on P and that β is very different from 1 might cast some shadows

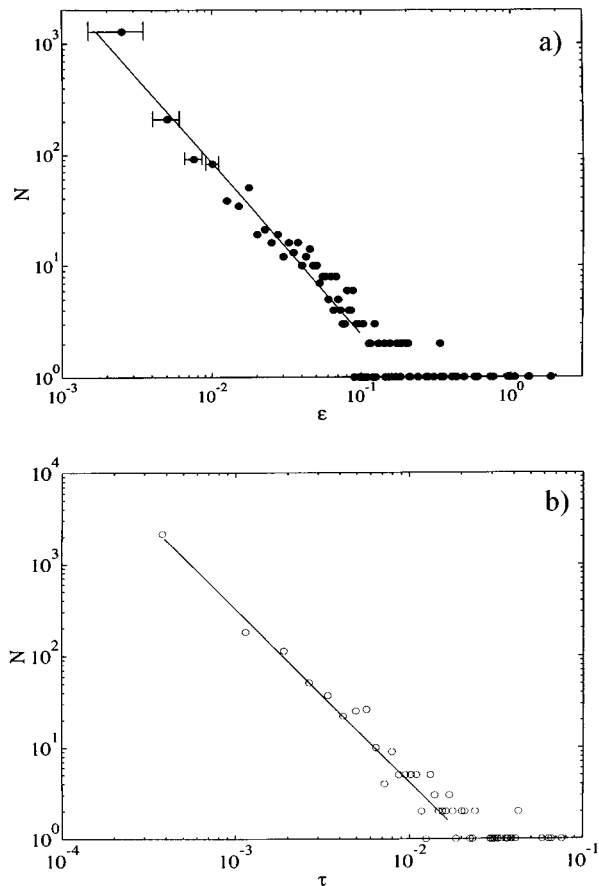


Fig. 8. (a) Histogram of the energy of AEs recorded in one sample. The solid line is a power fit of exponent $\gamma = 1.51$. (b) Histogram for the time interval τ between events. The solid line is a power fit. The average and standard deviation for the exponent calculated from 20 wood samples is 1.9 ± 0.1 .

on the eventual description of fracture in the framework of self-organized criticality (SOC). However the comparison between SOC and our result is not straightforward because SOC prescribes that the statistics of a SOC system should be studied at a constant value of the control parameter, whereas our exponents are obtained during a very slow sweep of P .

5 Kaiser effect

In 1950 Kaiser discovered that the AE of a stressed metal sample is zero if the applied stress is smaller than the maximum previously applied one [41]. This effect, usually called “Kaiser Effect”, was also discovered in rock materials [42,43], but its existence was seriously questioned for the Westerley Granite by Sondergeld and Estey in 1981 [44]. A good knowledge of this effect is very important because it can be very useful to know the maximum stress to which a material has been submitted in the past. In order to verify the validity of the Kaiser Effect on heterogeneous materials we applied a cyclic-load to our samples. As an example in Figure 9a the stress applied to the sample

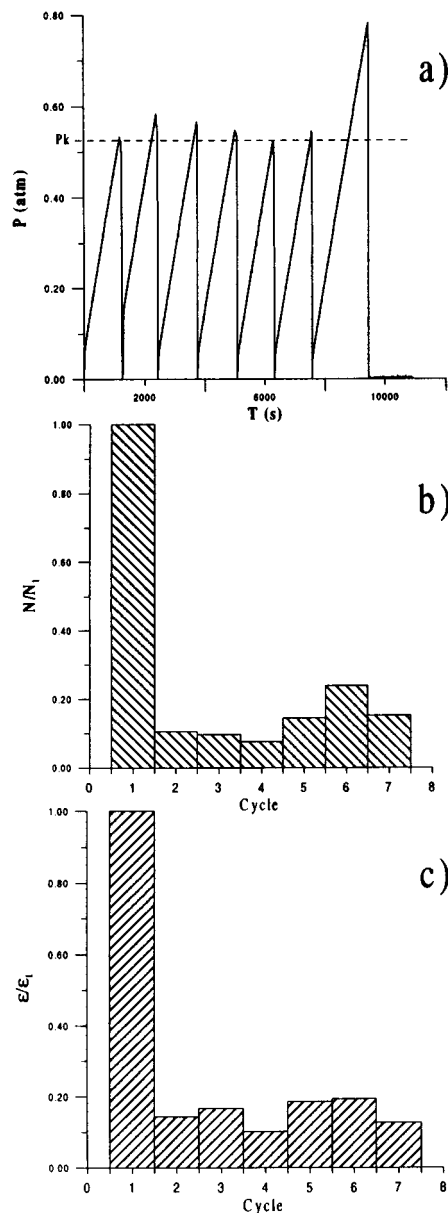


Fig. 9. (a) Imposed Pressure as a function of time. Definition of the Kaiser pressure P_k . (b) Number of events, normalized to the value obtained in the first cycle, as function of the cycle number. (c) Energy released, normalized to the one obtained in the first cycle, as a function of the cycle number. For all the cycles, only the events detected at $P < P_k$ are taken into account in this figure.

is plotted as a function of time. We see that 7 cycles are applied and the seventh is used to break the sample. We define the Kaiser pressure P_k as the minimum among the maximum pressure of the cycles. In Figures 9b and 9c the number of events N and the energy E detected in the different cycles and normalized to the values of the first cycle, are plotted as a function of the cycle number n_c . In Figures 9b and 9c for all the cycles, the last one included, *i.e.* the one which breaks the sample, only the events detected at $P < P_k$ are considered. We find that

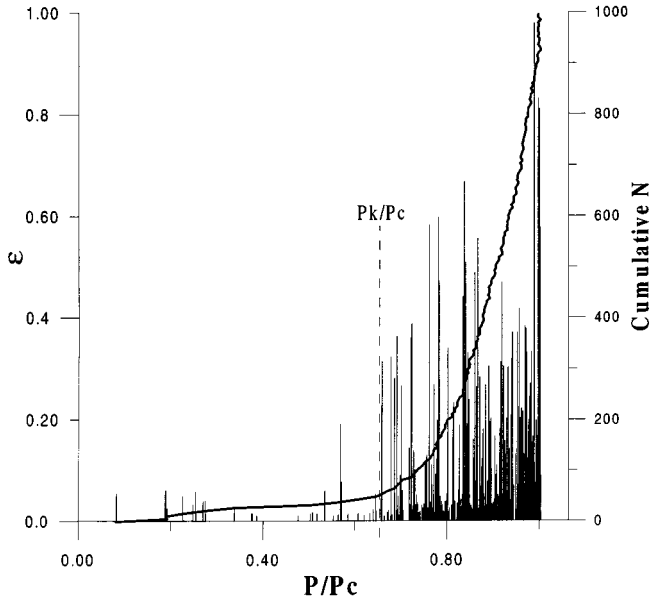


Fig. 10. Normalized energy bursts from AE and the cumulative number of events (continuous line) as a function of the normalized pressure, recorded during the last loading cycle.

from the second cycle on, N and ε are about the 15% of the value found during the first cycle. The AE of the last cycle is plotted as a function of P/P_c in Figure 10. We notice that when P_k is reached, the AE goes back to the usual behaviour. This means that all parameters revert to the measured behaviour explained in the previous paragraph. For instance, the same critical exponent and the same energy distribution is found. The sample forgets initial cycling load. We made those experiments for the case of imposed pressure. For the measures presented here we are not able to state what exactly happens to entropy during the cycles because of the little number of events after the first one and because we are not able to localize all of them. Looking at Figure 9, it seems that for the heterogeneous materials the Kaiser effect is not strictly valid. We can rule out the hypothesis that the events measured after the first cycle are caused by environmental and electrical noise. Indeed the trigger level of the AE acquisition system is always setted above the noise level and during a cycle we have at most 1% of events due to the noise. The events can be caused by new microcracks, by the shear of different parts of the samples during the deformation or by both. In Figure 11 the energy distribution of the first cycle and the mean energy distribution of the others cycles are plotted. We find two power laws with the same exponent. Also the dependence of the energy and the numbers of events as a function of the pressure is the same for the first cycles and for the others. These results point that the events occurred for the cycles after the first are caused by new microcracks. Shearing events, *i.e.* events caused by the shear of different parts of the samples, would result in behaviours of E and N as a function of pressure different from those due to microcracks. The spatial distribution of shearing events would be the union of little parts of

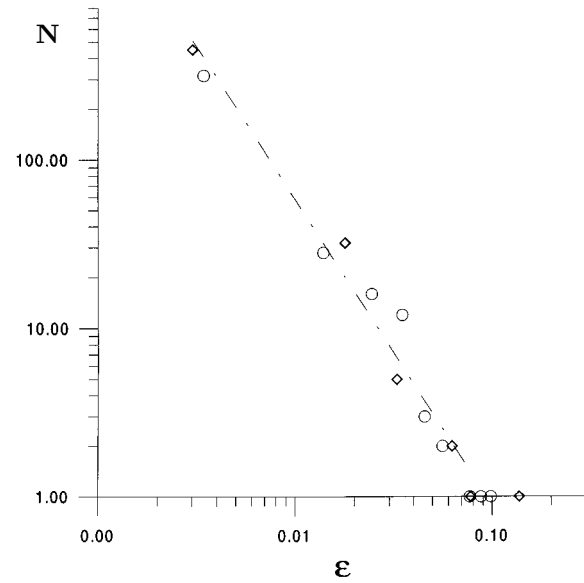


Fig. 11. Histograms of the energy of AEs recorded during the first cycle (squares) and the sum of the energy released during the other cycle (circles) when the pressure is less then P_k . The solid line is a power fit.

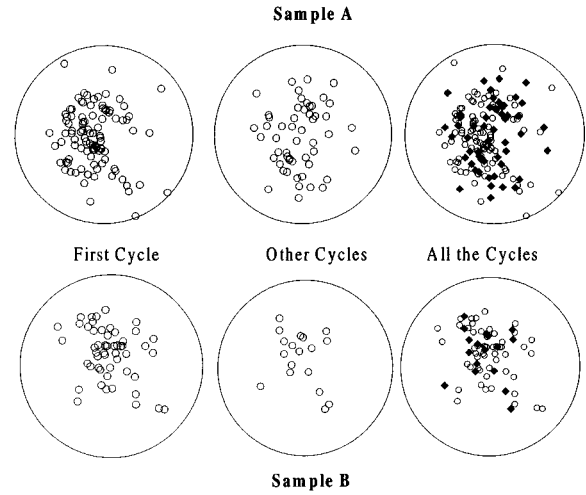


Fig. 12. The localization of microfractures for two different samples. Left column: the events occurred during the first cycle. Middle column: The events occurred during the other cycles at pressure $< P_k$. Right column: the superposition of all the microfractures occurred at pressure $< P_k$ during the first cycle (circles) and during the others (solid squares).

space with high density of events. The events of the cycles after the first one that we have been able to localize, Figure 12, are distributed all over the sample. So we can conclude that the events are caused by new microcracks. The entropy during the cycles after the first seems to be constant. This fact is coherent and reinforce the validity of the non-destructive test we proposed before. In conclusion, the Kaiser effect for the heterogeneous materials is not strictly valid, indeed we have a non-negligible number of new microcracks when we submit the sample below

a stress previously applied. However, this effect can be successfully used to investigate the stress history of a sample. Measuring the entropy of the new microcracks, one could know how the maximum stress, at which the sample has been submitted in the past, is close to the critical stress.

6 Conclusions and discussion

We have presented experimental data on the fracture of heterogeneous materials. One of the main motivation of this work was the comparison between the experimental results on the fracture heterogeneous materials and models such as percolation in a fuse network. These models are certainly an over-simplification of reality, furthermore they are more equivalent to mode III loading whereas our experiment is more close to mode I (see Sect. 2.4). However it is remarkable the strong qualitative and quantitative analogy of our results with those observed in numerical simulations of these models. The monitoring of acoustic emissions allows us to study the microfractures occurring before the final crack. We have shown that these precursors are more closely clustered as failure approaches. The formation of clusters near failure is independent on the loading procedure, showing that at least on a qualitative level percolation could be a good model for crack propagation. A measure of the concentration of microcracks may provide practical knowledge about the degree of damage suffered by the material. This method should be improved to render better predictions; it could be done, for example, by lowering the detection threshold of microfractures; it is likely that a higher number of events would give more accurate values. Improvements in the localization accuracy would also contribute. Besides, other measures of microfracture concentration could be tested

We have also show that the energy of acoustic emissions is a good characteristic parameter of the system to compare with the above models such as percolation in a fuse network. We have shown that under certain conditions (namely, that the loading is carried out at imposed stress) the behavior of energy allows us to consider fracture as a critical phenomenon, as displayed notably by the existence of a power law divergence near failure and by the statistical distributions of different variables. The lack of quantitative agreement between the exponents found in the experiment and those calculated in simulations of the above mentioned models is not surprising, given that particular factors (such as geometry) strongly influence their values. The relevant point is that brittle fracture in heterogeneous materials is amenable to be described in those frameworks. We have also shown that the Kaiser effect is not strictly valid in heterogeneous materials. However, this effect can be used to investigate the stress history of a sample of the material.

This work has been partially funded by Projects Nos. ER-BCHRXT940546 and ERBFMBICT950126 from the European Community. We acknowledge enlightening discussions with R. Livi, A. Politi and S. Roux, and we thank L. Bellon, J.F. Boudet and Y. Alm eras for their helpful comments.

The technicians of the ENSL have provided us technical aid. A. Garcimart ın thanks the European Community and the Spanish Government for a grant.

References

1. M.F. Kanninen, C.H. Popelar, *Advanced Fracture Mechanics* (Oxford University Press, NewYork, 1985).
2. L.B. Freund, *Dynamic Fracture Mechanics* (Cambridge University Press, Cambridge, 1990).
3. B. Lawn, *Fracture of Brittle Solids*, 2nd ed. (Cambridge University Press, Cambridge, 1993).
4. L.D. Landau, E.M. Lifshitz, *Theory of elasticity, Course of Theoretical Physics* (Pergamon, London, 1959), Vol. 7.
5. See for example M. Marder, J. Fineberg, *Phys. Today* **49**, 24 (1996).
6. J. Fineberg, S.P. Gross, M. Marder, H.L. Swinney, *Phys. Rev. B* **45**, 5146 (1992); J.F. Boudet, S. Ciliberto, V. Steinberg, *Europhys. Lett.* **30**, 337 (1995).
7. O.B. Naimark, V.V. Silberschmidt, *Eur. J. Mech. A Solids* **10**, 607 (1991).
8. E. Bouchaud, *J. Phys.-Cond.* **9**, 4319 (1997).
9. A. Hansen, E.L. Hinrichsen, S. Roux, *Phys. Rev. Lett.* **66**, 2476 (1991).
10. G. Perrin, J.R. Rice, *J. Mech. Phys. Solids* **47**, 1047 (1994).
11. W.T. Ashurst, W.G. Hoover, *Phys. Rev. B* **14**, 1465 (1976).
12. S.J. Zhou, D.M. Bearzley, P.S. Lomdahl, B.L. Holian, *Phys. Rev. Lett.* **78**, 479 (1997); S.J. Zhou, A.E. Carlson, R. Thomson, *Phys. Rev. Lett.* **72**, 852 (1994).
13. M. Marder, *Nature* **386**, 219 (1997), and references therein.
14. P. Espa ol, I. Z u iga, M.A. Rubio, *Materials Research Society symposium Proceedings* edited by R.L. Blumberg Selinger, J.J. Mecholsky, A.E. Carlsson, E.R. Fuller Jr. (Materials Research Society, Pittsburgh, 1996), Vol. 409.
15. L. De Arcangelis, H.J. Herrmann, *Phys. Rev. B* **39**, 2678 (1989); L. De Arcangelis, H. Hansen, H.J. Herrmann, S. Roux, *Phys. Rev. B* **40**, 877 (1989).
16. D. Sornette, C. Vanneste, *Phys. Rev. Lett.* **68**, 612 (1992).
17. H.J. Herrmann, S. Roux, *Statistical models for the fracture of disordered media* (North-Holland, Amsterdam, 1990).
18. P. Bak, C. Tang, K. Wiesenfeld, *Phys. Rev. Lett.* **59**, 381 (1987); *Phys. Rev. A* **38**, 364 (1988).
19. A. Garcimart ın, A. Guarino, L. Bellon, S. Ciliberto, *Phys. Rev. Lett.* **79**, 3202 (1997).
20. C.J. All gre, J.L. Le Mouel, A. Prevost, *Nature* **297**, 47-49 (1982).
21. R.F. Smalley, D.L. Turcotte, S.A. Solla, *J. Geophys. Res.* **90**, 1894 (1985).
22. A.A. Pollock, *International Advances in Nondestructive Testing*, **7**, 215-239 (1981).
23. A. Sornette, D. Sornette, *Tectonophysics* **179**, 327-334 (1990).
24. M. Enoki, T. Kishi T., *Int. J. Fracture* **38**, 295 (1988); K. Yul, W. Sachse, *J. Appl. Phys.* **65**, 4234 (1989).
25. K. Aki, P.G. Richards, *Quantitative seismology: Theory and methods* (W.H. Freeman & Co., San Francisco, 1980).
26. S.P. Timoshenko, S. Woinowsky-Krieger, *Theory of plates and shells*, 2nd ed. (McGraw-Hill, Engineering Mechanics Series, New York, 1959).
27. D. Lockner D., *Int. J. Rock Mech. Min. Sci. Geomech. Abstr.* **30**, 883 (1993).

28. D.A. Lockner, J.D. Byerlee, V. Kuksenko, A. Ponomarev, A. Sidorin, *Nature* **350**, 39 (1991).
29. R. López-Ruiz, H.L. Mancini, X. Calvet, *Phys. Lett. A* **209**, 321 (1995).
30. A. Sornette, P. Davy, D. Sornette, *J. Geophys. Res.* **98**, 12111-12139 (1993).
31. A.O. Hero, O. Michel, *International Symposium on Information Theory*, Ulm, Germany, 1997 (in press).
32. P. Diodati, F. Marchesoni, S. Piazza, *Phys. Rev. Lett.* **67**, 2239 (1991).
33. G. Cannelli, R. Cantelli, F. Cordero, *Phys. Rev. Lett.* **70**, 3923 (1993).
34. A. Petri, G. Paparo, A. Vespignani, A. Alippi, M. Constantini, *Phys. Rev. Lett.* **73**, 3423 (1994).
35. J.-C. Anifrani, C. Le Floc'h, D. Sornette, B. Souillard, *J. Phys. I France* **5**, 631 (1995).
36. M.A. Muñoz, G. Gristein, R. Dickman, R. Livi, *Phys. Rev. Lett.* **76**, 451 (1996); *Physica D* **103**, 485 (1997).
37. K. Chen, P. Bak, S.P. Obukhov, *Phys. Rev. A* **43**, 625 (1991).
38. D. Turcotte, *Fractal and Chaos in Geology* (Cambridge University Press, 1992).
39. P.C. Hemmer, A. Hansen, *J. Appl. Mech.* **59**, 909 (1992); M. Kloster, A. Hansen, P.C. Hemmer, Burst avalanches in solvable models of fibrous materials, preprint.
40. A. Sornette, D. Sornette, *Europhys. Lett.* **9**, 197 (1989).
41. J. Kaiser, Ph.D. thesis, Tech. Hosch. Munchen, Munich (1950).
42. K. Kurita, N. Fujii, *Geophysical Res. Lett.* **6**, 9 (1979).
43. T. Kanagawa, M. Hayashi, H. Nakasa, *Estimation of the spatial Geo-Stress component in Rock samples using the Kaiser effect of acoustic emission*, Tech. Report, C.R.I.E.P.I., E375004 (1976).
44. C. Sondergeld, L. Estey, *J. Geophys. Res.* **86**, 2915 (1981).